(Received 12 February 2026, Accepted 6 March 2026, Scheduled 3 April 2026)

A High-Selectivity 3-D Dual-Polarized Frequency Selective Rasorber with Wide Absorption Bands Based on Multiple Strip-Type Resonators

Hao Shen[1,2], Borui Bian[1,2,*], and Dan Zhang[1,2]

[1] School of Information Science and Technology, Nanjing Forestry University, Nanjing 210037, China
[2] School of Artificial Intelligence, Nanjing Forestry University, Nanjing 210037, China

ABSTRACT: This letter presents a high-selectivity three-dimensional (3-D) dual-polarized frequency-selective rasorber (FSR). The proposed design comprises a 3-D array of multiple lossy strip-type resonators integrated with a planar bandpass frequency-selective surface (FSS). While the multiple resonances of the strips provide wideband absorption, a parallel LC structure is loaded within each resonator to achieve a low-loss transmission band. Numerical and experimental results demonstrate an ultra-wide low-reflection band with a fractional bandwidth (FBW) of 162.2% from 2.0 to 19.2 GHz. This includes a transmission band at 10 GHz with an insertion loss of 0.47 dB, alongside a lower frequency absorption band (2.0–9.5 GHz, FBW 130.4%) and an upper frequency absorption band (10.5–19.2 GHz, FBW 58.6%). The operating mechanism is further validated by an equivalent circuit model and measurement of a fabricated prototype, showing good agreement between theory and experiment.

1. INTRODUCTION

The design of a frequency-selective rasorber (FSR) is one of the most attractive techniques in target stealth engineering. Because it can substantially absorb out-of-band signals, the FSR can potentially replace the traditional frequency-selective surface (FSS) to achieve out-of-band bi-static radar cross section reduction (RCSR) for antenna or radar systems [1].

Currently, there are two main design approaches for constructing FSR structures. The first is the conventional two-dimensional (2-D) structural design. 2-D FSRs are typically realized by constructing a specially designed lossy layer above a bandpass FSS. The absorption performance depends on the lossy layer, which is usually achieved by loading appropriate lumped resistors onto unit cells [2–22]. By introducing parallel resonances, a passband with a low insertion loss can be achieved either outside [3, 9, 11, 13] or within [2, 4–8, 10, 12, 14–17] the absorption band. Although reported 2-D FSR designs are usually low-profile, low-cost, and easily dual-polarized, their relatively narrow absorption bandwidth and large periodicity are their main practical limitations.

The other approach to FSR design is based on three-dimensional (3-D) FSSs. By independently constructing transmission and absorption paths, some outstanding 3-D FSR designs have been developed [23–31]. The transmission path, usually realized by an open-circuited parallel-plate waveguide (PPW) section loaded with a metallic post at the center, produces a passband with a sharp roll-off performance [23]. The absorption path, which can be implemented by loading the lumped resistors at appropriate locations in a short-circuited PPW section, provides a one- or two-sided absorption band around the passband. Recent research has focused on integrating lossy layers with FSSs [24–31] to overcome the fundamental limitations of traditional absorbers. This combined approach is pivotal for achieving broadband absorption to suppress radar signatures while maintaining high-selectivity windows for signal transmission. Owing to the additional design dimension and smaller unit cell, 3-D FSRs can achieve excellent performance, such as higher selectivity and better angular stability. Nevertheless, the relatively narrow absorption bandwidth is the main practical challenge in applying 3-D FSRs, and the complicated 3-D topology limits their implementation in arrays and dual-polarized applications.

While recent 3-D frequency-selective rasorbers (FSRs) exhibit excellent filtering performance, they often suffer from complex spatial topologies and relatively narrow absorption bandwidths, which limit their implementation in dual-polarized and large-scale applications. To overcome these limitations, we propose a new 3-D FSR based on an orthogonally interlocked printed circuit board (PCB) topology. By integrating the structural features of existing 2-D and 3-D FSR designs, our proposed structure significantly simplifies the fabrication process while achieving an ultra-wide absorption band and stable dual-polarization capability. The main contributions of the proposed 3-D FSR are summarized as follows:

1. By introducing multiple resonances into the 3-D structure, the proposed FSR achieves an ultra-wide low-reflection band with a -10 dB fractional bandwidth (FBW) of 162.2% from 2.0 to 19.2 GHz. Two wide absorption bands (absorptivity $>$ 90%) span from 2.0 to 9.5 GHz (130.4% FBW) and from 10.5 to 19.2 GHz (58.6% FBW), respectively.

* Corresponding author: Borui Bian (bbr@njfu.edu.cn).

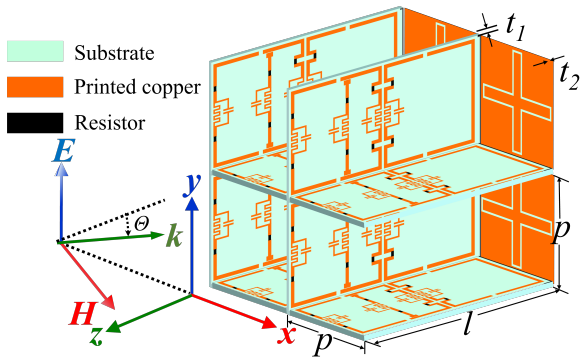

FIGURE 1. Geometrical structure of the proposed 3-D FSR unit cells (2×2 array). (Dimensions in mm: $p = 11.308$, $l = 21.5$, $t_1 = 0.508$, $t_2 = 0.25$.).

2. Owing to the simple construction of interlocked PCB elements etched with multiple strip resonators and a bottom planar metallic bandpass FSS, the proposed 3-D FSR design significantly simplifies dual-polarized implementation and fabrication processes.

2. DESIGN AND DISCUSSION

2.1. Structure of the Proposed 3-D FSR

The geometrical structure of the proposed 3-D FSR unit cell is illustrated in Fig. 1. The FSR consists of an array of 3-D hollow symmetric structures backed by a planar FSS ground plane. The top 3-D hollow structure comprises PCB elements etched with multiple resistor-loaded strip resonators, which are interlocked orthogonally in both the vertical and horizontal directions. Owing to this orthogonal configuration, the PCB elements are independently responsible for TE and TM polarizations. For the planar backplane, a slot-type cross-frame-shaped FSS is employed, providing dual-polarized reflective and transmissive performance. In this design, Rogers TMM4 ($\varepsilon_r = 4.5$, $\tan\delta = 0.002$) and F4B ($\varepsilon_r = 2.65$, $\tan\delta = 0.003$) substrates were used for the top hollow structure and the bottom FSS layer, respectively.

Figure 2 presents the geometrical details of a single PCB and FSS element within a unit cell. Four separate U-shaped metallic strips were etched in series from the top to the bottom of the PCB element, with a straight strip positioned between the two incident-side U-type strips. To achieve the desired absorptivity, two resistors were loaded along the edges of the three incident-side U-type strips and the straight strip. Furthermore, a parallel LC resonator was integrated into the center of each resistor-loaded strip, comprising a meandering line and a parallel strip acting as the inductor and capacitor, respectively. Additionally, the slot-type cross-frame element serves as a bandpass FSS, exhibiting polarization-insensitive transmission and ultra-wide out-of-band reflection, thereby acting as an effective ground plane for absorption. By matching the resonant frequency of the parallel LC structure with the passband of the FSS, the proposed FSR achieves a highly-selective transmission window with a low insertion loss.

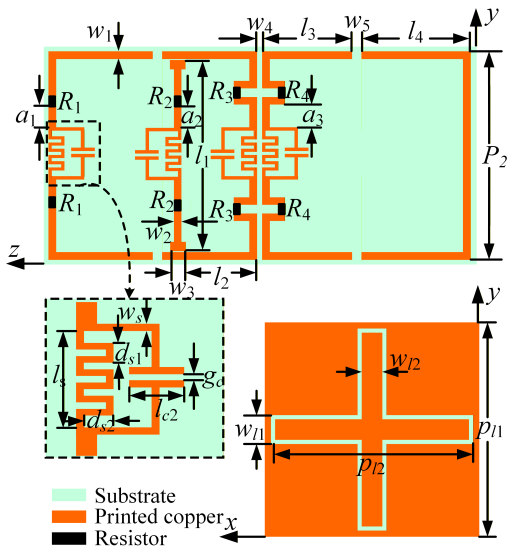

FIGURE 2. The geometrical details of a PCB structure and the unit cell of the FSS. (Physical dimensions (mm): $p_1 = 10.6$, $a_1 = 0.8$, $a_2 = 1.4$, $a_3 = 1.3$, $w_1 = 0.25$, $w_2 = 0.25$, $w_3 = 0.7$, $w_4 = 0.1$, $w_5 = 0.2$, $l_1 = 9.85$, $l_2 = 3.8$, $l_3 = 4.7$, $l_4 = 5.7$, $l_s = 1.9$, $l_c = 0.7$, $w_s = 0.15$, $g_c = 0.1$, $d_{s1} = 0.35$, $d_{s2} = 0.8$, $pl_1 = 11.308$, $pl_2 = 7.5$, $wl_1 = 1.2$, $wl_2 = 0.9$. Lumped resistors: $R_1 = 430\,\Omega$, $R_2 = 200\,\Omega$, $R_3 = 300\,\Omega$, $R_4 = 350\,\Omega$.).

2.2. 3-D Ultra-Wideband (UWB) Absorber

Similar to the tailoring methodology of the reported 3-D FSRs, the construction of a 3-D Ultra-Wideband (UWB) absorber is the fundamental building block for the proposed 3-D FSR design. Fig. 3 illustrates the proposed 3-D UWB absorber. In the unit cell, four in-series U-type strips and a straight strip are etched on two cross-inserted PCB pieces backed by a PEC

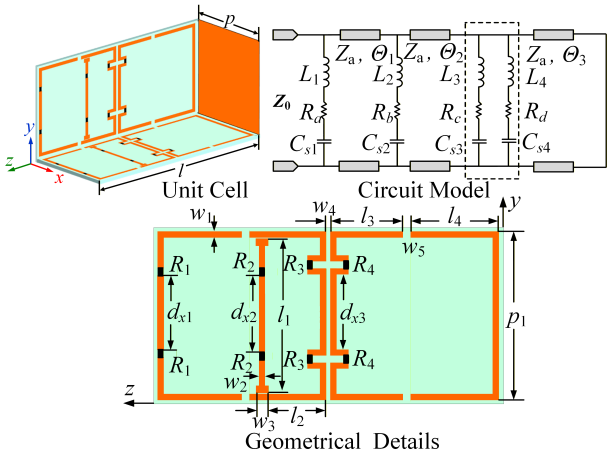

FIGURE 3. Illustration of the proposed 3-D UWB absorber and its equivalent circuit model. (Physical dimensions (mm): $p = 11.308$, $l = 21.5$, $w_1 = 0.25$, $w_2 = 0.25$, $w_3 = 0.7$, $w_4 = 0.1$, $w_5 = 0.2$, $p_1 = 10.6$, $l_1 = 9.85$, $l_2 = 5.3$, $l_3 = 4.7$, $l_4 = 5.7$, $dx_1 = 4.75$, $dx_2 = 5.325$, $dx_3 = 6.625$. Lumped resistors: $R_1 = 430\,\Omega$, $R_2 = 200\,\Omega$, $R_3 = 300\,\Omega$, $R_4 = 350\,\Omega$. Circuit parameters: $R_a = 860\,\Omega$, $R_b = 400\,\Omega$, $R_c = 600\,\Omega$, $R_d = 700\,\Omega$, $L_1 = 7.04$ nH, $L_2 = 2.4$ nH, $L_3 = L_4 = 6.1$ nH, $C_{s1} = 38$ fF, $C_{s2} = 260$ fF, $C_{s3} = C_{s4} = 34$ fF, $Z_0 = Z_a = 377\,\Omega$, $\Theta_1 = 23.4^\circ$ at 3 GHz, $\Theta_2 = 15.3^\circ$ at 3 GHz, and $\Theta_3 = 38.7^\circ$ at 3 GHz).

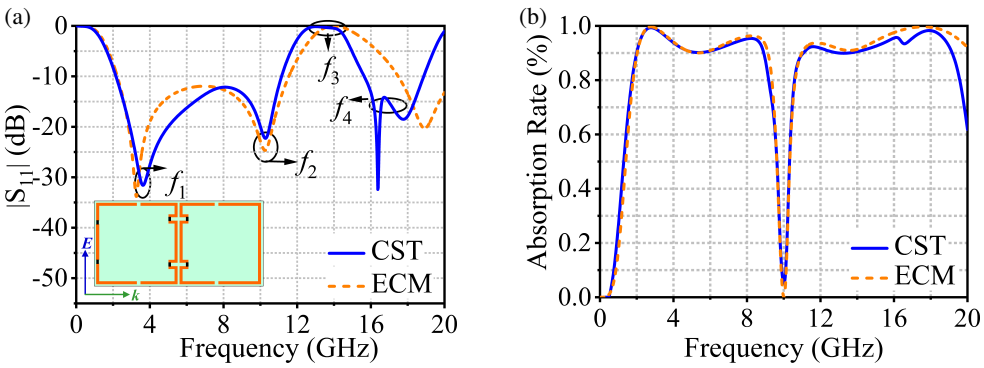

FIGURE 4. The reflection results of the original and proposed absorbers under normal incidence obtained by CST and ECM. (a) Original absorber; (b) Proposed absorber.

ground plane. Three near-source U-type strips and a straight strip provide the desired absorption at certain frequencies. To effectively dissipate the incident power along the strips for better absorption performance, two resistors were inserted along each edge of the strips.

Here, we employ a similar 3-D absorber structure but without etching the lossy straight strips, referred to as the "original absorber." The reflection results of the original and proposed absorbers under normal incidence for TE polarization (E along the y axis, $\theta = 0°$), simulated by CST Microwave Studio, are shown in Fig. 4. The original absorber exhibited an absorption-reflection-absorption frequency response. A perfect reflection band with a reflection coefficient $|S_{11}| = 1$ at approximately 14 GHz and two-sided wide absorption bands with an absorption rate of more than 90% were achieved. The two absorption bands are realized at 2.1–11.1 GHz (136.3% FBW) and 15.6–18.9 GHz (19.1% FBW), respectively. Notably this original absorber with a reflection band has potential applications in antenna out-of-band RCSR if it is used as a ground plane or reflector in an antenna system.

Furthermore, by loading appropriate lossy straight strips into suitable locations of the unit cell, the impedance of the original absorber can be made to match the characteristic impedance of free space within the reflection band. Hence, the desired UWB absorber can be realized using this design. As shown in Fig. 4(b), the proposed absorber exhibits an ultra-wide low-reflection band with a -10 dB FBW of 162% from 1.94–18.5 GHz. The total thickness was $0.14\lambda_L$ at its lowest absorption frequency.

The equivalent circuit model (ECM) of the proposed absorber is presented in Fig. 3, and its circuit includes four series RLC resonators and a short-circuited transmission-line (TL) section consisting of three cascaded TL subsections with different electrical lengths (Θ_1, Θ_2, and Θ_3, where $\Theta_3 = \Theta_1 + \Theta_2$). The inductors ($L_1, L_3, L_4$, and L_2) denote the inductances of the U-type strips and the straight strip, respectively. C_{S1}, C_{S3}, and C_{S4} denote the coupling capacitors between the U-type strips of adjacent unit cells along the direction of the electric field. C_{S2} is the coupling capacitor between the straight strip and the neighboring U-type strip in the unit cell. The resistors (R_a, R_b, R_c, and R_d) denote the equivalent resistance values of each strip.

For the original absorber, corresponding to the circuit excluding the series $R_bL_2C_{s2}$ resonator, the absorption band has resonant frequencies f_1, f_2, and f_4, and the reflection band is around f_3, as shown in Fig. 4(a). It is easy to calculate that, at f_1, the total electrical length Θ_t ($\Theta_t = 2\Theta_3$) of the short-circuited TL section corresponds to a quarter wavelength, and the resonant frequency of the $R_aL_1C_{s1}$ resonator is designed around f_1. In this case, the equivalent impedance of the original absorber is close to the pure resistive value R_a, $|S_{11}|$ approaches zero; thus, substantial absorption can be achieved. At f_2 and f_4, since Θ_t corresponds to three-quarter wavelengths at f_2 and five-quarter wavelengths at f_4, the absorptions at these two resonant frequencies are the harmonic responses of the $R_aL_1C_{s1}$ resonator. Furthermore, at f_3, where Θ_t is equal to half the wavelength, the loaded resistors are bypassed by the short-circuited air TL resonator, and the equivalent impedance of the original absorber approaches zero (short circuit condition). Thus, a perfect reflection band with $|S_{11}| = 1$ was produced around f_3. In addition, by loading $R_cL_3C_{s3}$ and $R_dL_4C_{s4}$ circuits at the electrical length Θ_3 of the short-circuited TL resonator, which corresponds to a quarter wavelength of approximately 6.5 GHz, good impedance matching can be achieved between f_1 and f_2.

For the proposed absorber, to achieve the desired UWB absorption performance, an $R_bL_2C_{s2}$ circuit is loaded between the $R_aL_1C_{s1}$ and $R_cL_3C_{s3}$ circuits. The corresponding electrical length $\Theta_a(\Theta_a = \Theta_2 + \Theta_3)$ of the short-circuited TL resonator is equal to three-quarter wavelengths at f_3. By optimizing the equivalent impedance with suitable resistance, inductance, and capacitance, good impedance matching can be achieved around f_3, resulting in an ultra-wide absorption performance. The reflection results of the absorbers under normal incidence calculated by the ECM are also presented in Fig. 4, and it can be seen that the ECM results agree well with the full-wave simulation results.

2.3. 3-D Dual-Polarized FSR

In the conventional 3-D FSR design approach, a transmission path is usually constructed in parallel with the unit cell of the absorber along the polarization direction, and a series LC resonator is loaded in front of the unit cell to short-circuit the absorber at the passband frequencies for low insertion-loss trans-

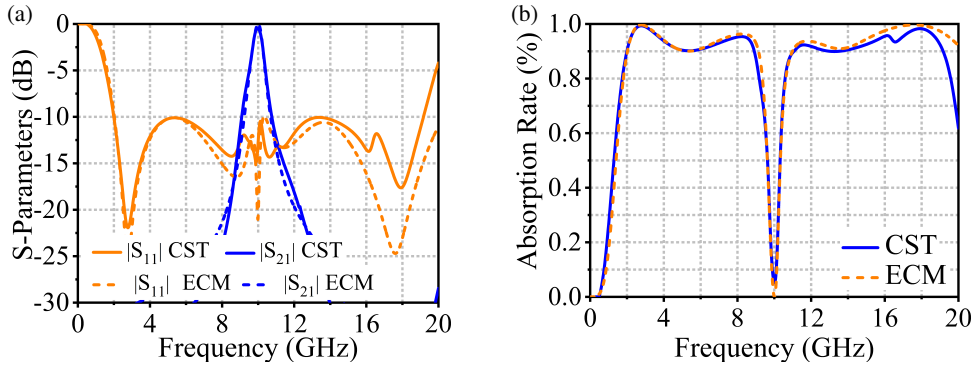

FIGURE 5. The performance of the proposed FSR under normal incidence obtained by CST and ECM. (a) S-parameters; (b) Absorption rate.

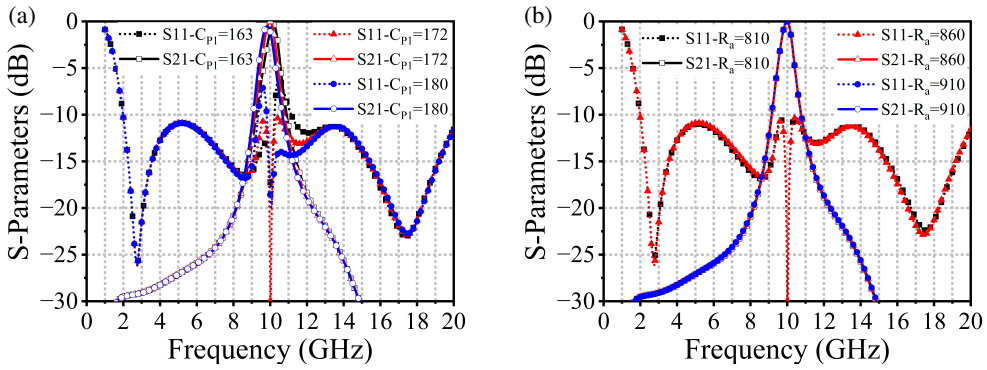

FIGURE 6. Sensitivity analysis of the equivalent circuit model (ECM). (a) Simulated frequency responses under varying parallel capacitance C_{p1} (163 fF, 172 fF, and 180 fF); (b) Simulated absorption responses under varying equivalent resistance R_a (810 Ω, 860 Ω, and 910 Ω).

mission. Here, based on the proposed 3-D UWB absorber design, the transmission path is constructed by adding parallel LC structures to multiple series RLC resonators to produce infinite impedance, and by replacing the PEC ground plane with a slot-type cross-frame-shaped bandpass FSS. In contrast to existing 3-D FSR approaches, this design not only maintains the compact dimensions of the unit cell but also reduces the manufacturing complexity. The proposed 3-D dual-polarized FSR structure is illustrated in Fig. 1.

The simulated S-parameters and absorption rate of the proposed 3-D dual-polarized FSR under normal incidence for TE polarization obtained by CST are shown in Fig. 5. It can be seen that the FSR has an ultra-wide low-reflection band at 2.0–19.2 GHz with a -10 dB FBW of 162.2%. Two absorption bands with absorption rates of $\geq$ 90% are realized at 2.0–8.9 GHz (126.6% FBW) and 11–19.2 GHz (54.3% FBW). Meanwhile, it exhibits a highly selective transmission band with the lowest insertion loss of 0.47 dB at 10 GHz.

To further evaluate the robustness of the proposed equivalent circuit model, a sensitivity analysis of critical ECM parameters was conducted. As depicted in Fig. 6(a) and Fig. 6(b), we investigated the influence of varying the parallel capacitance C_{p1} and the equivalent resistance R_a by approximately $\pm$5%. Specifically, C_{p1} was swept across 163 fF, 172 fF (the nominal value), and 180 fF, while R_a was evaluated at 810 Ω, 860 Ω (the nominal value), and 910 Ω. The analysis demonstrates that the variation in C_{p1} causes a slight shift of less than 0.2 GHz in the transmission frequency, and the variation in R_a results in negligible degradation in the absorption band. These parametric sweeps confirm the strong robustness of the established circuit model against minor modeling or manufacturing perturbations.

Based on the ECM of the previously analyzed UWB absorber, the ECM of the proposed FSR was constructed as shown in Fig. 7. Four identical parallel circuits ($L_{p1}C_{p1}$), which denote the parallel LC structures, are added to the four series RLC resonators. The added parallel resonance can provide infinite impedance for the series RLC circuit and guarantee that the resistors are isolated for a low-insertion-loss transmission. In addition, the ECM (L_{p2}, L_{s2}, C_{p2} and C_{s5}) representing the slot-type cross-frame-shaped FSS functions as a spatial bandpass filter characterized by a broad reflection band. Due to the geometric complexity of the 3-D interlocked structure, the specific ECM parameter extraction relies on a hybrid approach. The initial values of the LC components were first estimated using simplified analytical formulas for periodic arrays. Subsequently, these initial parameters were modeled in Advanced Design System (ADS) software, where a curve-fitting optimization algorithm was utilized to fine-tune the final circuit parameters to achieve a high correspondence with the full-wave simulation S-parameters. The impedance of the FSS equivalent circuit approaches zero and infinity in the reflection and transmission bands, respectively. When the circuit operates in the reflection band, a wideband absorption performance is achieved, similar to the characteristics of the previously ana-

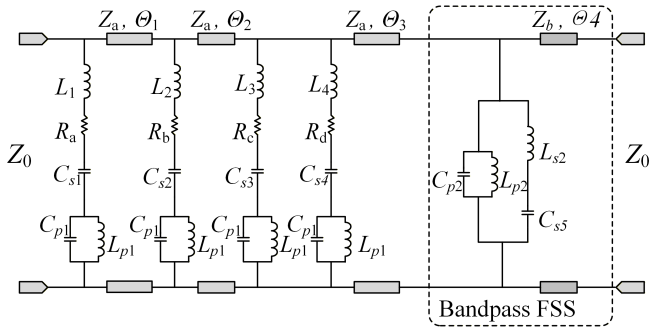

FIGURE 7. The ECM of the proposed FSR. Circuit parameters: $R_a = 860\,\Omega$, $R_b = 400\,\Omega$, $R_c = 600\,\Omega$, $R_d = 700\,\Omega$, $L_1 = 6.24\,\text{nH}$, $L_2 = 1.6\,\text{nH}$, $L_3 = L_4 = 5.3\,\text{nH}$, $L_{p1} = 1.48\,\text{nH}$, $L_{p2} = 0.52\,\text{nH}$, $L_{s2} = 0.3\,\text{nH}$, $C_{s1} = 38\,\text{fF}$, $C_{p1} = 172\,\text{fF}$, $C_{s2} = 260\,\text{fF}$, $C_{s3} = C_{s4} = 38\,\text{fF}$, $C_{p2} = 93\,\text{fF}$, $C_{s5} = 265.6\,\text{fF}$, $Z_0 = Z_a = 377\,\Omega$, $Z_b = 231.5\,\Omega$, $\Theta_1 = 23.4^\circ$ at 3 GHz, $\Theta_2 = 15.3^\circ$ at 3 GHz, $\Theta_3 = 38.7^\circ$ at 3 GHz and $\Theta_4 = 1.456^\circ$ at 3 GHz.

lyzed UWB absorber. When the circuit operates at the desired transmission frequency (10 GHz), which matches the resonant frequency of the added parallel LC circuits, the entire circuit model of the FSR appears open-circuited (high impedance in series arms), allowing the incident energy to pass through with a low insertion loss. The S-parameters and absorption rate of the proposed 3-D FSR obtained using the ECM are also shown in Fig. 5.

The S-parameters of the TE and TM polarizations under oblique incidence were also investigated, as shown in Fig. 8. Under TE-polarized oblique incidence, as the incidence angle θ increases to 30°, the absorption performance remains stable and the transmission characteristics are almost unchanged, although a slight degradation appears at the upper absorption band. Analogously, a stable absorption performance was observed under a TM-polarized oblique incidence. Although the transmission peak degraded slightly, the insertion loss remained less than 1 dB at an incidence of 30° incidence.Under oblique incidence, the slight discrepancy between TE and TM response curves arises because the free-space wave impedance changes differently with incident angle θ (shifting to $Z_0/\cos\theta$ for TE waves and $Z_0\cos\theta$ for TM waves), leading to varied impedance matching conditions.

3. MEASUREMENT AND DISCUSSION

To validate the designed 3-D FSR, a 3-D FSR prototype was fabricated and measured. A photograph of the fabricated prototype and its details are shown in Fig. 9. The prototype consisted of 10×10 unit cells with a total size of $215\,\text{mm} \times 215\,\text{mm} \times 21.5\,\text{mm}$. Two UWB horn antennas were used as transmitting and receiving antennas. Since the physical dimensions of the fabricated prototype are relatively small compared to the free-space wavelength at the lowest operating frequency, rigorous measures were taken to ensure measurement accuracy. Specifically, the prototype was surrounded by a substantial amount of commercial polyurethane foam absorbers to prevent spatial electromagnetic diffraction. Furthermore, the time-domain gating technique of the Vector Network Analyzer (VNA) was employed to effectively suppress any residual edge diffraction. The measurement setup is illustrated in Fig. 9(c).

The measured S-parameters of the proposed 3-D FSR under the normal incidence is plotted in Fig. 10(a). A relatively good agreement was observed between the measured and simulated results. As verified by full-wave simulations, the inherent PCB fabrication tolerance (± 0.05 mm) has a negligible impact on the overall performance. Therefore, the slight frequency shift of the transmission band and the minor perturbations in the curves are primarily attributed to unavoidable manual assembly alignment issues (e.g., microscopic air gaps) and measurement errors. The extracted absorption rate is also presented in Fig. 10(b). It can be seen that a measured -10 dB low-reflection band is achieved from 2.0 to 19.7 GHz (163% FBW), and a highly selective transmission band with an insertion loss of 0.62 dB is centered at 10.2 GHz. In addition, the lower and upper measured absorption bands with an absorption rate of $\geq$ 90% are achieved from 2.0 to 8.9 GHz (145% FBW) and from 11.7 to 19.7 GHz (51% FBW), respectively. The noise floor of the measurement system is approximately -45 dB, which is well below the lowest measured reflection levels, ensuring high data credibility. The measured -3 dB transmission bandwidth is restricted to only 0.64 GHz. From a physical perspective, this limitation stems from the fundamental trade-off governed by the single-stage parallel LC resonator utilized in the 3-D structure. To achieve the demonstrated high frequency selectivity with sharp roll-off skirts between the absorption and transmission bands, the resonator must operate with a high quality factor, which inherently limits its operational passband. Furthermore, the bottom layer employs a single-layer FSS that acts essentially as a single-pole bandpass filter, lacking the wideband flat-top response characteristics.

To demonstrate the advantages of the proposed FSR design, a comparison with existing FSR designs is presented in Table 1. The proposed 3-D FSR achieves significant improvements in the low-reflection bandwidth, absorption rate, and dual-polarization capability. However, a notable limitation of the current design is its relatively narrow transmission band. Physically, this narrow bandwidth fundamentally stems from

TABLE 1. Comparison with reported FSR designs.

Ref.	Type	FBW (%)	LAB (%)	UAB (%)	IL (dB)	Thickness (λ_L)	Pol.
[2]	2-D	120	75.2	35.5	0.16	0.12	Dual
[4]	2-D	142.5	96.3	48.6	0.38	0.13	Dual
[5]	2-D	122.8	59.9	29.6	1	0.074	Dual
[8]	2-D	139.4	92.5	58.8	0.48	0.1	Dual
[24]	3-D	156.9	120	43	0.4	0.118	Dual
[25]	3-D	73.8	48.8	27.7	N.A.	0.25	Single
[26]	3-D	46.2	N.A.	46.2	N.A.	0.36	Dual
[27]	3-D	135.6	42.3	45.1	1.05	0.108	Dual
Our work	**3-D**	**162.2**	**130.4**	**58.6**	**0.47**	**0.14**	**Dual**

FBW = fractional bandwidth of -10 dB reflection. LAB/UAB = lower/upper absorption bandwidth are for 90% absorption rate. IL = insertion loss. λ_L = free space wavelength at the lowest frequency of -10 dB reflection.

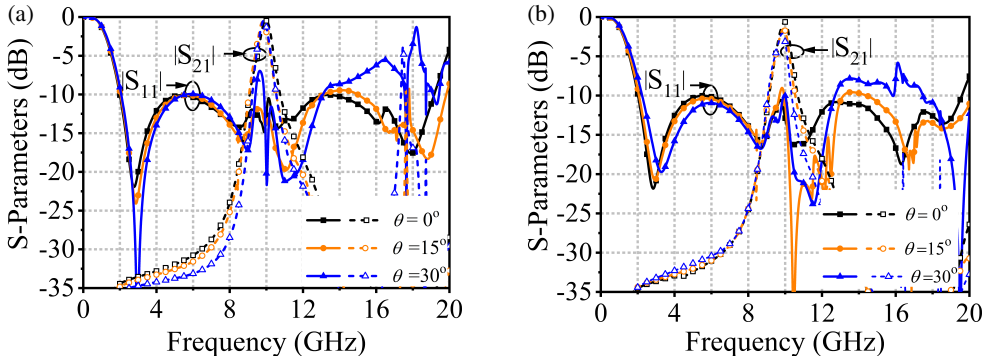

FIGURE 8. S-parameters of the proposed 3-D FSR under oblique incidence. (a) TE polarization. (b) TM polarization.

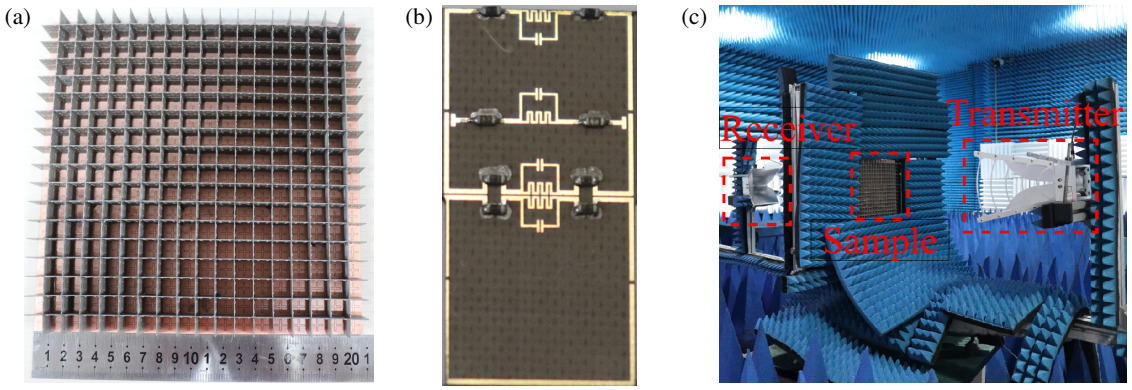

FIGURE 9. The prototype and measurement setup of the proposed 3-D FSR. (a) Photograph of the prototype. (b) Unit cell of the 3-D hollow structure. (c) Measurement setup.

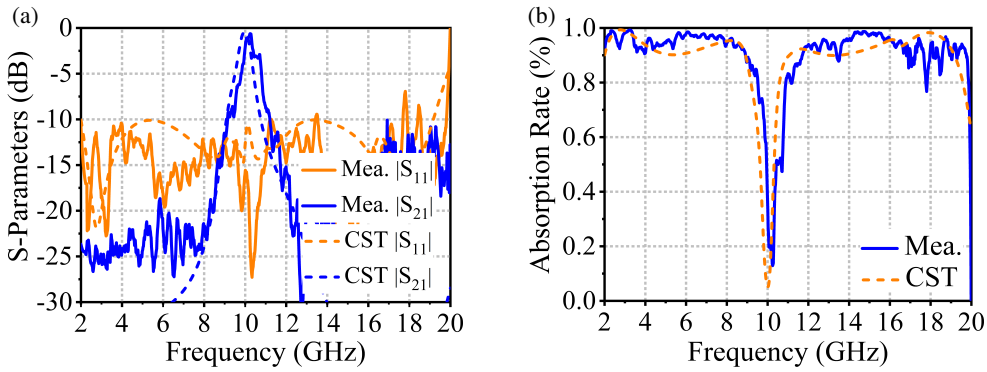

FIGURE 10. The performance of the proposed 3-D FSR under normal incidence obtained by CST and measurement. (a) S-parameters. (b) Absorption rate.

the single-stage resonance mechanism. The current transmission window is generated by a single parallel LC resonator coupled with a single-layer FSS ground, which inherently provides only a single transmission pole and results in a sharp, narrow resonance peak. To address this limitation and achieve a wider transmission window, future work could focus on two structural improvements: (1) cascading multiple parallel LC resonators in series to introduce multiple, closely spaced transmission poles, thereby yielding a wider, flat-top passband; and (2) employing a multi-layer or higher-order wideband bandpass FSS, instead of the current single-layer narrow bandpass FSS, to fundamentally expand the bandwidth limits of the transmission path.

4. CONCLUSION

By employing multiple strip-type resonators, a new 3-D dual-polarized FSR was proposed with an ultra-wide low-reflection FBW of 162.2%. Two wide absorption bands with absorptivity exceeding 90% were observed at the lower and upper frequency bands, respectively. By loading parallel LC structures and a planar bandpass FSS, a passband performance of approximately 10 GHz was achieved. Owing to the construction of cross-inserted PCB pieces etched with multiple planar resonators, the proposed 3-D FSR design significantly simplifies the fabrication process and naturally supports dual-polarized operation. An ECM was been introduced to elucidate the operating mecha-

nism of the FSR. Finally, the good agreement between the measured and simulated results demonstrates the feasibility of the proposed FSR design.

ACKNOWLEDGEMENT

This work was supported in part by the National Natural Science Foundation of China (Grant No. 62101266), Fundamental Research Funds for the Central Universities, Jiangsu Agriculture Science and Technology Innovation Fund (JASTIF; No. CX (21)3187), and the Project of Key Laboratory of Radar Imaging and Microwave Photonics, Ministry of Education of China under Grant RIMP2023005.

REFERENCES

[1] Munk, B. A., *Frequency Selective Surfaces: Theory and Design*, John Wiley & Sons, 2005.

[2] Zhang, Y., N. Kou, and S. Yu, "A broad band-pass frequency selective rasorber based on screen printed conductive ink," *IEEE Antennas and Wireless Propagation Letters*, Vol. 24, No. 10, 3505–3509, 2025.

[3] Wang, B., X. Ding, Y. Cai, Y. Wu, W. Li, Z. Luo, K. Si, Z. Cao, J. Jiang, and L. Miao, "A broadband dual polarization transmission frequency selective rasorber with low insertion loss," *IEEE Antennas and Wireless Propagation Letters*, Vol. 24, No. 9, 2754–2758, 2025.

[4] Xiong, J., Y. Wu, F. Deng, K. Wang, B. Yang, X. Shi, and H. Lin, "A dual-polarized frequency-selective rasorber with wideband switchable transmission/absorption capability," *IEEE Antennas and Wireless Propagation Letters*, 1–5, 2026.

[5] Macilon, R. D. S., A. G. D'Assuncao, V. P. D. S. Neto, A. G. D'Assunção, and C. J. O. Peixeiro, "A low-profile dual-polarized frequency-selective rasorber based on one-eighth wavelength spacer and interdigital resonator," *IEEE Access*, Vol. 13, 147 943–147 952, 2025.

[6] Xing, Z., J. Cui, P. Yang, Q. Wang, G. Yang, J. Li, and L. Wang, "Broadband transmission rasorber with dual-broadband absorption by high-accuracy equivalent admittance analysis method with convergent solution conditions," *IEEE Transactions on Electromagnetic Compatibility*, Vol. 67, No. 5, 1423–1431, 2025.

[7] Govindarajan, G., G. N. A. Mohammed, A. Premanand, M. Kanagasabai, and P. Bactavatchalame, "Design of miniaturized conformal rasorber using machine learning for precision intrusion mitigation," *IEEE Antennas and Wireless Propagation Letters*, Vol. 24, No. 9, 2849–2853, 2025.

[8] Ai, J., J. Hong, R. X.-K. Gao, C. Liu, X. Zhao, and L. Yan, "Enhanced equivalent circuit model-aided broadband single-lossy-single-lossless-layer rasorber design with high selectivity," *IEEE Antennas and Wireless Propagation Letters*, Vol. 24, No. 5, 1080–1084, 2025.

[9] Yu, Y., W. Yu, W. Wang, L. Liu, and G. Q. Luo, "Low-RCS ultra-wideband antenna based on bandabsorptive frequency selective rasorber," *IEEE Antennas and Wireless Propagation Letters*, Vol. 24, No. 12, 4680–4684, 2025.

[10] Jiang, H., Y. Zhang, Y. Wu, B. Jiang, S. Liao, and Q. Xue, "Reconfigurable bandpass frequency-selective rasorber with perfect elliptic filtering response," *IEEE Transactions on Microwave Theory and Techniques*, Vol. 73, No. 1, 423–435, 2025.

[11] Wang, Y., X. Jiang, P. K. Choudhury, and Y. Ma, "Temporally controlled switchable microwave rasorbers," *IEEE Antennas and Wireless Propagation Letters*, Vol. 24, No. 3, 577–581, 2025.

[12] Hao, W., W. Zhou, Z. Ye, S. Liu, and X. Ji, "Wideband reconfigurable frequency selective rasorber with absorption enhanced fusion bias network," *IEEE Transactions on Microwave Theory and Techniques*, Vol. 73, No. 10, 8083–8093, 2025.

[13] Chen, J., W. Yu, W. Wang, Q. Tan, L. Liu, and G. Q. Luo, "Polarization-independent switchable frequency selective rasorber based on parallel DC bias network," *IEEE Antennas and Wireless Propagation Letters*, Vol. 24, No. 4, 848–852, 2025.

[14] Kou, N. and S. Yu, "Wide harmonic-band absorbed frequency selective rasorber with enhanced angular stability based on equivalent circuit synthesis," *IEEE Transactions on Electromagnetic Compatibility*, Vol. 65, No. 6, 1952–1959, 2023.

[15] Wang, Y., X. Jiang, P. K. Choudhury, and Y. Ma, "Toward reconfigurable two-bit microwave chiral rasorbers," *Progress In Electromagnetics Research M*, Vol. 130, 83–94, 2024.

[16] Kumar, A., G. Sen, and J. Ghosh, "Design of a compact SRR loaded polarization-independent wideband meta-material rasorber with a narrow transmission window," *Progress In Electromagnetics Research M*, Vol. 131, 37–44, 2025.

[17] Lin, L., J. Zhang, L. Li, X. Li, and Q. Wang, "A frequency selective rasorber with ultra-wideband switchable transmission/reflection and two-sided absorption," *Progress In Electromagnetics Research M*, Vol. 133, 1–9, 2025.

[18] Geng, J., X.-H. Deng, Z. Xiong, J. Gao, B. Song, and Y. Lou, "A metasurface capable of simultaneous stealth across multiple electromagnetic wave bands and its design concept," *Composites Communications*, Vol. 55, 102328, 2025.

[19] Geng, J., X.-H. Deng, Z. Xiong, J. Gao, and B. Song, "Innovative design to achieve a multi-band electromagnetic wave stealth," *Optics Letters*, Vol. 49, No. 18, 5328–5331, 2024.

[20] Geng, J., X.-H. Deng, Z. Xiong, J. Gao, B. Song, and J. Yuan, "Ultra-wideband terahertz absorber with switchable multiple modes based on graphene and vanadium dioxide metamaterials," *Chinese Journal of Physics*, Vol. 92, 1312–1324, 2024.

[21] Lou, Y., X.-H. Deng, J. Geng, S. Zhu, Y. Liu, Y. Zhang, Y. Bao, and P. Hu, "Design of metasurface structures compatible with multiple detection methods for stealth applications," *Physics Letters A*, Vol. 544, 130487, 2025.

[22] Khani, A. A. M., A. B. Haghverdi, I. Rezaei, S. J. H. Zoljalali, and T. Aghaee, "Tunable graphene-based wave absorber: Combined electrical and mechanical tuning," *Smart Wearable Technology*, 1–7, 2025.

[23] Li, M. and Z. Shen, "Hybrid rasorber based on 3-D bandpass frequency-selective structures," *IEEE Antennas and Wireless Propagation Letters*, Vol. 23, No. 12, 4882–4886, 2024.

[24] Chen, J., W. Yu, Y. Chen, X. Zhang, L. Liu, and G. Q. Luo, "A switchable frequency-selective rasorber with wide transmission/absorption bands and sharp roll-off characteristics," *IEEE Transactions on Microwave Theory and Techniques*, Vol. 73, No. 12, 10 190–10 198, 2025.

[25] Zou, Y., X. Kong, Z. Hou, L. Wang, Q. Chen, Y. Zhao, F. Costa, and S. Gao, "A wideband amplifying frequency selective rasorber based on a 2.5-D antenna-circuit-antenna structure," *IEEE Transactions on Antennas and Propagation*, Vol. 73, No. 8, 5600–5609, 2025.

[26] Yu, Y., C. Zhang, Q. Liu, Z. Liao, and L. Peng, "High-selectivity band-absorptive frequency-selective rasorber," *IEEE Antennas and Wireless Propagation Letters*, Vol. 23, No. 9, 2623–2627, 2024.

[27] Zhong, S., J. Feng, Z.-W. Zheng, and Y. Ma, "Ultrathin and simple 3-D rasorber based on ferrites with embedded epsilon-near-zero waveguides," *IEEE Antennas and Wireless Propaga-*

tion Letters, Vol. 21, No. 9, 1896–1900, 2022.

[28] Omar, A. A., H. Huang, and Z. Shen, "Absorptive frequency-selective reflection/transmission structures: A review and future perspectives," *IEEE Antennas and Propagation Magazine*, Vol. 62, No. 4, 62–74, Aug. 2020.

[29] Huang, H., Z. Shen, and A. A. Omar, "3-D absorptive frequency selective reflector for antenna radar cross section reduction," *IEEE Transactions on Antennas and Propagation*, Vol. 65, No. 11, 5908–5917, 2017.

[30] Wang, L., S. Liu, X. Kong, H. Zhang, Q. Yu, and Y. Wen, "Frequency-selective rasorber with a wide high-transmission passband based on multiple coplanar parallel resonances," *IEEE Antennas and Wireless Propagation Letters*, Vol. 19, No. 2, 337–340, 2020.

[31] Wang, D., X. Cui, D. Liu, X. Zou, G. Wang, B. Zheng, and T. Cai, "Multi-characteristic integrated ultra-wideband frequency selective rasorber," *Progress In Electromagnetics Research*, Vol. 179, 49–59, 2024.